We are IntechOpen, the world's leading publisher of Open Access books Built by scientists, for scientists

4,800
Open access books available

122,000
International authors and editors

135M
Downloads

Our authors are among the

154
Countries delivered to

TOP 1%
most cited scientists

12.2%
Contributors from top 500 universities

WEB OF SCIENCE™

Selection of our books indexed in the Book Citation Index in Web of Science™ Core Collection (BKCI)

Interested in publishing with us?
Contact book.department@intechopen.com

Numbers displayed above are based on latest data collected.
For more information visit www.intechopen.com

3

Microstructure, Diffusion and Growth Mechanism of Nb_3Sn Superconductor by Bronze Technique

Aloke Paul[1], Tomi Laurila[2] and Vesa Vuorinen[2]
[1]*Department of Materials Engineering, Indian Institute of Science, Bangalore -560012*
[2]*Electronics Integration and Reliability, Department of Electronics, Helsinki University of Technology, FIN-02015 TKK*
[1]*India*
[2]*Finland*

1. Introduction

Nb-Ti is a widely used superconductor material. However, its use is limited to applications of magnetic field upto 8T (Sharma, 1987). At the present, Nb_3Sn intermetallic compound with A15 structure is considered to be one of the most suitable superconductors for the applications where field requirements go beyond the limit of Nb-Ti superconductors. However, intermetallic compounds are in general brittle and cannot be drawn as wire. To circumvent this problem, different manufacturing technologies have been developed for Nb_3Sn, such as bronze method, internal tin process, powder metallurgy route, Jelly roll process, ECN technique (Suenaga, 1981; Sharma, 1987) etc.
In this chapter, we shall discuss mainly the growth and diffusion mechanism of Nb_3Sn fabricated by the bronze technique. In this method, several Nb rods are inserted inside Cu(Sn) bronze alloy and drawn as a multifilamentary wire. The product phase Nb_3Sn is grown during the subsequent annealing by solid state diffusion. The efficiency of a superconductor wire largely depends on the presence of microstructural defects, such as grain boundaries and Kirkendall pores, grain size distribution, the variation of chemical composition over the cross section (Suenaga, 1981; Suenaga & Jansen, 1983; Lee & Larbalestier, 2005; Lee & Larbalestier, 2008) and so on. The application of pure Nb_3Sn compound has been found to be limited to magnetic fields of 12 T, since the increase in the field drastically reduces the critical current density, J_c. Further improvements have been achieved by alloying Nb_3Sn with different elements, such as Ti, Ta, Zr, Mg etc. (Suenaga et al., 1986). Thus, the aim of this chapter is to discuss and analyse various factors which affect the growth of the product phase by diffusion controlled process. The evolution of microstructure is detemined by the thermodynamics and kinetics of the system. The combined thermodynamic-kinetic approach will be discussed, which provides a feasible tool to rationalize the formation of the observed reaction structures.

2. Microstructural aspects

Grain boundaries play an important role on flux pinning and thus the critical current density is strongly influenced by the grain size distribution in a given multifilamentary

structure. Typical grain structure is shown in Fig. 1 (Flükiger et al., 2008). As explained by Müller & Schneider, 2008, mainly two different grain morphologies can be distinguished. Near the Nb core columnar grains are typically found, whereas near the Cu(Sn) bronze alloy equiaxed grains are generally seen. Further there can exist two types of equiaxed grains: small grains in the middle of the Nb_3Sn layer and coarse grains near to the Cu(Sn) alloy. Average grain size, as shown in Fig. 2, is found to increase with annealing time and temperature. However the average grain size does not define the distribution unambiguously, as shown in Fig. 3.

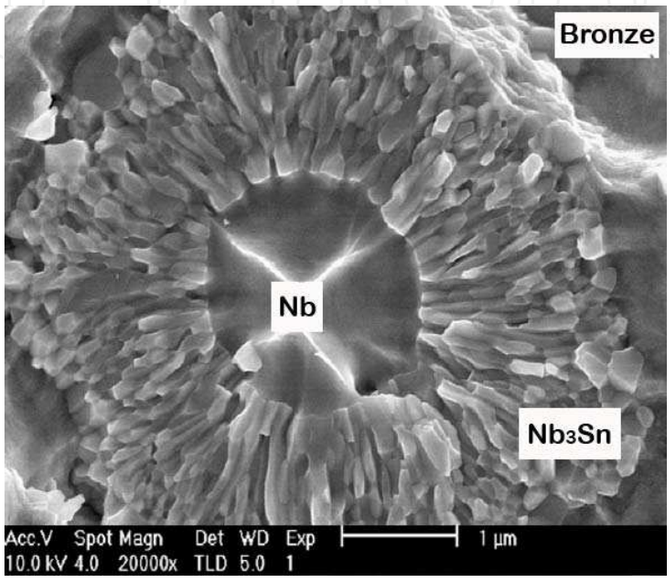

Fig. 1. Grain morphology of Nb_3Sn layer (Flükiger et al., 2008).

3. Diffusion mechanism

In the bronze technique, Nb rods are embedded in Cu(Sn) bronze alloy. Sn concentration in the alloy, in general, is kept within the solid solubility range of 6-8 at.%Sn in Cu. The composite structure is then drawn as a wire with the required dimensions. Subsequently, the multifilamentary wire is annealed in the temperature range of 600-800 ^{o}C. Nb_3Sn grows as product layer at the Cu(Sn)/Nb interface by interdiffusion process. The overall physical and mechanical properties of the structure depend on the thickness, composition and morphological evolution of the product phase (Suenaga, 1981; Sharma, 1987). Morphological evolution in the interdiffusion zone depends on many factors. Among them are the annealing temperature and time, relative mobilities of the species, number of nucleation sites and so on. Further increase in the grain size along with the growth of the product layer makes the whole process very complicated. It has also been reported that Kirkendall pores are formed near the Nb_3Sn/Cu(Sn) interface. This indicates that there must be a significant difference in the mobilities of the species (Sn and Nb) through the product layer. Vacancies flow opposite to the direction of the faster diffusing species and in general get consumed by different sites those act as sink, such as the edge dislocations, grain boundaries and interfaces. However, in some systems, because of unavailability of sufficient sites as sink, vacancies coalescence and form pores (Adda & Philibert, 1981). It can easily be understood

that the presence of pores can adversely affect the overall performance of the structure. The position of the pores indicates that Sn must be the faster diffusing species through the product phase. Cu is not considered to contribute to the growth process, since its concentration in Nb_3Sn is generally found to be negligible. This issue should, however, be confirmed, in order to better understand the interdiffusion behavior in Nb_3Sn.

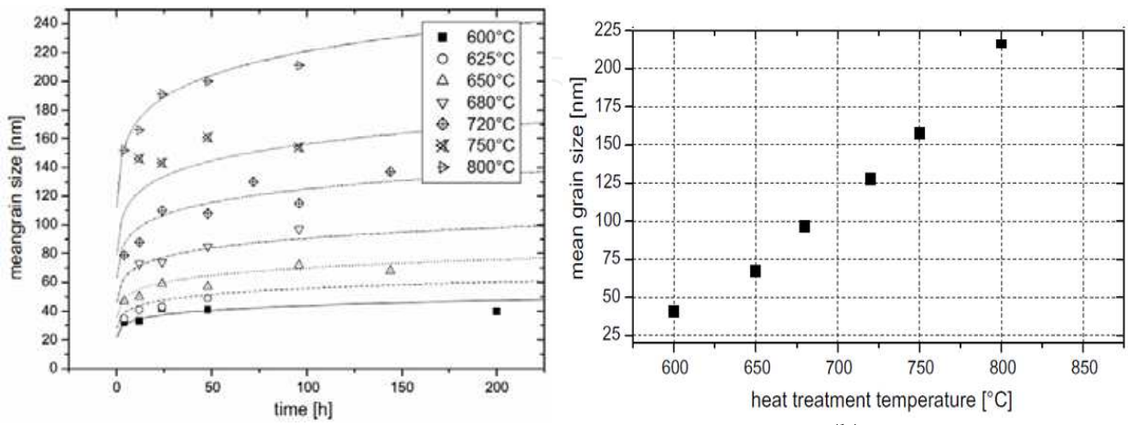

(a) (b)

Fig. 2. (a) The change in average grain size with the increase in annealing time at different temperatures is shown. (b) The increase in average grain size with temperature after fixed annealing time of 100 h is shown (Müller & Schneider, 2008).

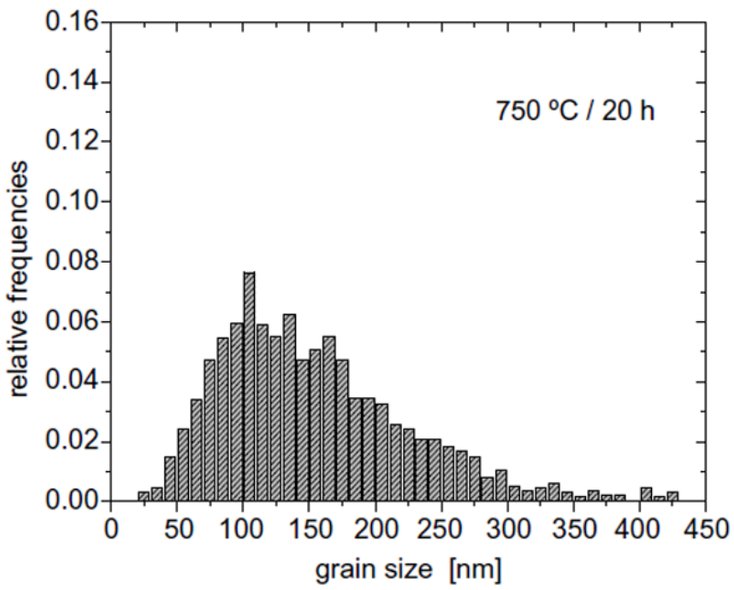

Fig. 3. Grain size distribution after annealing for 20 h at 750 °C (Müller & Schneider, 2008).

Hence, understanding the diffusion process is very important, since it is a key factor (together with thermodynamics) in the formation of microstructure, which ultimately controls the performance of the material. There are numerous studies published in order to understand the growth and diffusion mechanisms of Nb_3Sn, after the bronze method was developed to produce the superconductors (Sharma, 1987). However, the basic

understanding of the diffusion process is still lacking. This is not surprising since many times it is extremely difficult to draw any conclusion about the exact diffusion mechanism from simple diffusion couple experiments. Both lattice and grain boundary diffusion can be operative simultaneously and it is almost impossible to find the exact contribution from different mechanisms. To get rough idea about the diffusion mechanism, experiments are typically conducted at a particular temperature to measure the growth exponent. As stated earlier (Harrison, 1961), when the diffusion process is mainly controlled by lattice (Type A-kinetics) or grain boundary diffusion (Type C-kinetics), growth exponent is found to be of the order of 0.5. When contribution comes from lattice and grain boundary diffusion simultaneously, growth exponent is typically found to be around 0.25 (Type B-kinetics). Another way to evaluate the diffusion mechanism is by calculating the activation energy for diffusion by utilizing the Arrhenius equation. In general it is found that the activation energy for grain boundary diffusion is relatively low, since atoms need to cross the migration barrier only. On the other hand, the activation energy for lattice diffusion is found to be much higher, since the activation barrier for formation and migration of defects is added to the activation energy.

Several studies have concentrated in determining the growth exponent to evaluate the diffusion mechanism. For example, Farrel et al. (Farrel et al., 1974; Farrel et al., 1975) prepared multifilamentary wire by inserting Nb rods in the Cu(5at.%Sn) alloy. The rods were subsequenmtly drawn as wire with an approximate individual filament diameter of 25 μm. Multifilamentary wires were first annealed at two different temperatures, 700 and 800 ◦C for different annealing times to determine growth exponent. They noticed that layer was very wavy in nature. This is clear from the standard deviation of the average layer thickness shown in Fig. 4a. They found that the growth exponent is around 0.35±0.02. They also measured the temperature dependence of the growth of the phase in order to calculate the activation energy for diffusion, as shown in Fig. 4b. Activation energy was found to be around 12.4 kcal/mole (51.9 kJ/mol). Further study was conducted with higher Sn concentration in the bronze alloy and it showed that the growth rate becomes more sensitive to the Sn concentration starting from 7 at.%Sn and the growth exponent increases with increasing Sn concentration. Further, the growth rate became linear after certain annealing time, when bronze alloy had around 11.5 at.%Sn. As this is already beyond the solubility range of Sn in Cu, this result should be taken to be only indicative. They also found cracks in the Nb_3Sn phase after certain thickness. It was explained that the growth rate becomes linear because of the presence of cracks.

Reddi et al. (Reddi et al., 1983) carried out more systematic experiments to determine the change in the growth exponent along with the change in Sn concentration in the bronze alloy as well as a function of annealing temperature. Sn concentration was varied in the range of 2.01 to 10.87 wt.% (1.09 – 6.1 at.%). The diameter of the individual Nb rods in the multifilamentary wire was 0.12 mm. Experiments were conducted in the temperature range of 650–850 ◦C for 9 to 225 hrs. They reported that at 700 ◦C, growth exponent changes from 0.87 to 0.57 with the increase in Sn concentration from 7.29 to 10.87 wt.%. At 750 ◦C, as shown in Fig. 5a, the same changes from 0.80 to 0.57 with the change in Sn concentration from 3.30-10.87 wt.%. At 800 ◦C, as shown in Fig. 5b, it changes from 0.90 to 0.65 with the change in Sn concentration from 2.01-8.36 wt.%. They further noticed, as shown in Fig. 6a that the growth exponent mainly depends on the Sn concentration in the bronze alloy and more or less insensitive to the annealing temperature, as shown in Fig. 6b. The values were

further compared with the data available in the literature. They also calculated the activation energy for growth for the sample with 7 wt.%Sn (3.87 at.%) in the bronze alloy and found the value of 230 kJ/mol. It should be noted that this value is much higher than the value determined by Farrel et al. (Farrel et al., 1974). This is rather close to the value of 215-225 kJ/mol calculated by Larbalestier et al. (Larbalestier et al., 1975).

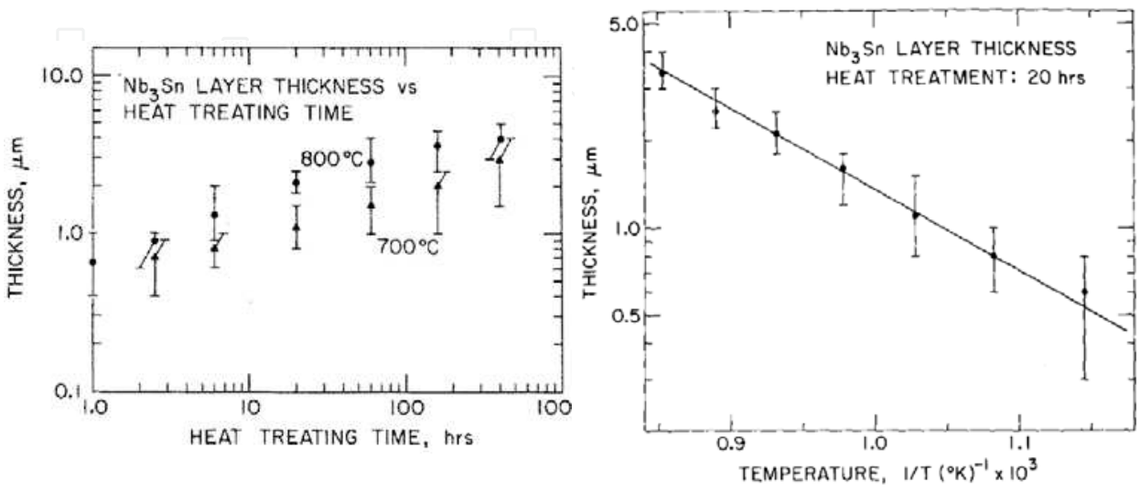

(a) (b)

Fig. 4. (a) The increase in layer thickness with annealing time at two different temperatures and (b) the layer thickness at different annealing temperatures, as reported by Farrel et al., 1974 and Farrel et al., 1975 are shown.

A more recent study (Muranishi & Kajihara, 2005) investigated the growth of the Nb_3Sn phase in the temperature range of 650-780 ◦C. They considered only 8.3 at.%Sn in the bronze alloy. They conducted experiments with diffusion couple technique with planar interfaces. There is an important difference between this and the earlier studies as will be discussed later on. Unlike the result of Reddi et al. (Reddi et al., 1983), they found that growth exponent is different at different temperatures. In the range of 650-700 ◦C, the growth exponent was found to be around 0.96 and decreased to 0.77 at 780 ◦C.

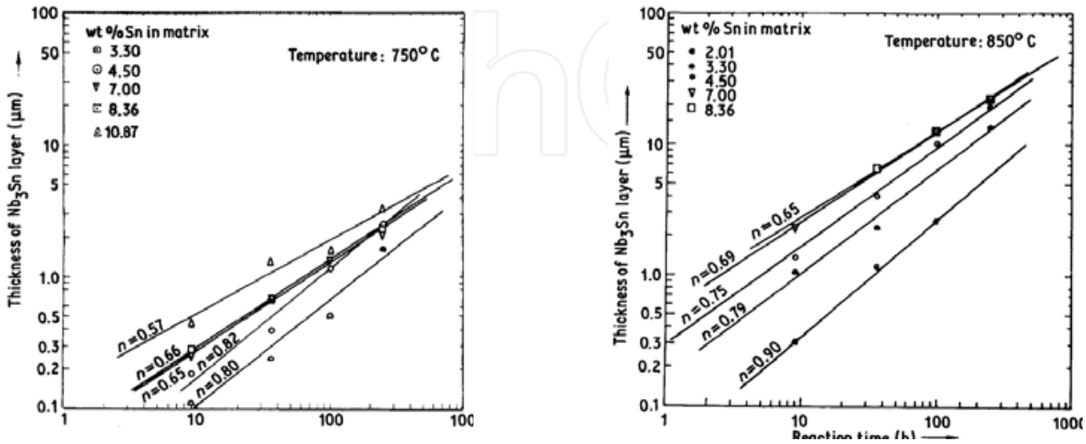

Fig. 5. The increase in layer thickness with annealing time and growth exponent at (a) 750 ◦C and (b) 850 ◦C as reported by Reddi et al., 1983 is shown.

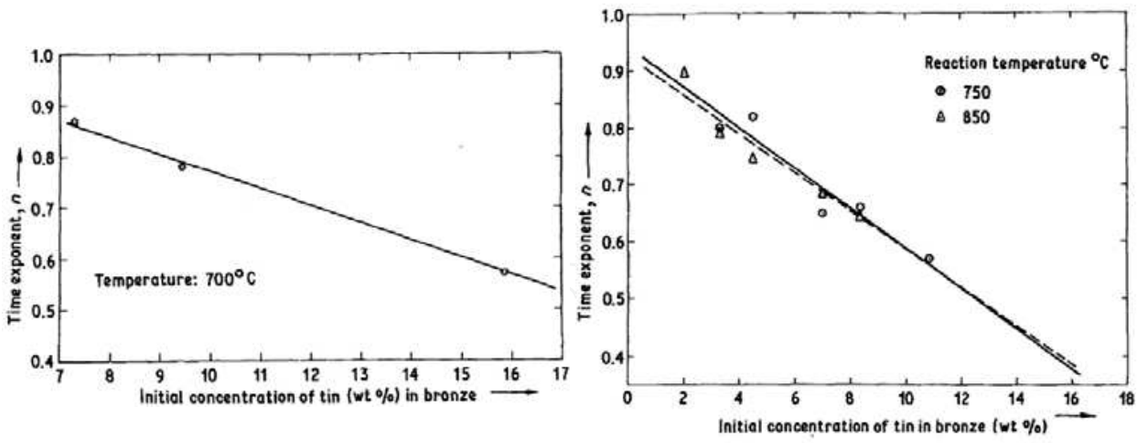

(a) (b)

Fig. 6. The variation of growth exponent with respect to Sn concentration in bronze alloy at (a) 700 ◦C and (b) 750 and 800 ◦C as reported by Reddi et al. is shown (Reddi et al., 1983).

What has been stated above clearly shows that it is very difficult to draw definite conclusions about the growth exponent of the Nb_3Sn phase. Outcome of different studies is found to be very different from each other. Further, a very common problem was found in most of the studies. To imitate the actual structure, experiments were mainly conducted with multi or monofilamentary structure, where Nb rods are surrounded by Cu(Sn) bronze alloy. However, the studies applied the growth kinetic relations derived for the sample geometries with planar interface. It should be noted that interdiffusion study with this geometry is rather complicated compared to the interdiffusion process in a specimen with planar interface. It is also not possible to use the laws developed for planar interface directly in the experimental results that are achieved from the experiments with cylindrical geometry, since the growth rate in this condition does not follow the same relation (van Loo, 1990). In a diffusion couple with planar interface, interfacial area does not change. However in a diffusion couple with cylindrical geometry, interfacial area continuously changes with the annealing time, as shown in Fig. 7a and growth deviates from linearity when plotted Δx vs. $\sqrt{t}$ as shown in Fig. 7b. Moreover because of waviness in the layer thickness, standard deviation is found to be very high. So it is very difficult to determine the exact growth exponent. Very few interdiffusion studies with planar interface have been reported (Muranishi & Kajihara, 2005; Hayase & Kajihara, 2006).

It is typically considered that Sn is virtually the only diffusing species through the product phase in the Nb/Cu(Sn) system. This is not an bad assumption, since the Kirkendall pores, which are formed because of unequal mobilities of the species, are found near the Cu(Sn)/Nb_3Sn interface (Easton & Kroeger 1979). This indicates that Sn must be the fastest diffusing species through the product layer.

To quantify the relative mobilities of the species during the growth of Nb_3Sn, Kirkendall marker experiments were carried out by Kumar & Paul (Kumar & Paul, 2009). Bronze alloys with the composition of 7 and 8 at.%Sn were prepared to couple with pure Nb. These compositions were selected, since according to Reddi et al. (Reddi et al., 1983) growth exponent was found to be close to 0.5, when Sn concentration in the bronze alloy was relatively high. After melting the alloys in an induction furnace in vacuum (~10^{-6} mbar), samples were annealed at 700 ◦C in vacuum for 48 h to achieve better homogeneity. The

average composition was further monitored by electron dispersive X-ray spectrometer (EDX). The experiments were conducted with planar interface geometry. TiO_2 particles of around 1 μm size were introduced at the initial contact plane, which acted as the inert Kirkendall markers. Experiments were done at three different temperatures of 700, 750 and 775 °C for 100-330 h. The cross-section from the (Cu-8at.%Sn)/Nb diffusion couple annealed at 775 °C for 330 h is shown in Fig. 8a. The composition profile measured by EDX is shown in Fig. 8b. Inert particles were found at the Cu(Sn)/Nb interface. Since the amount of Cu in the Nb_3Sn phase was negligible, it can be said that Sn is virtually the only mobile species through the product phase.

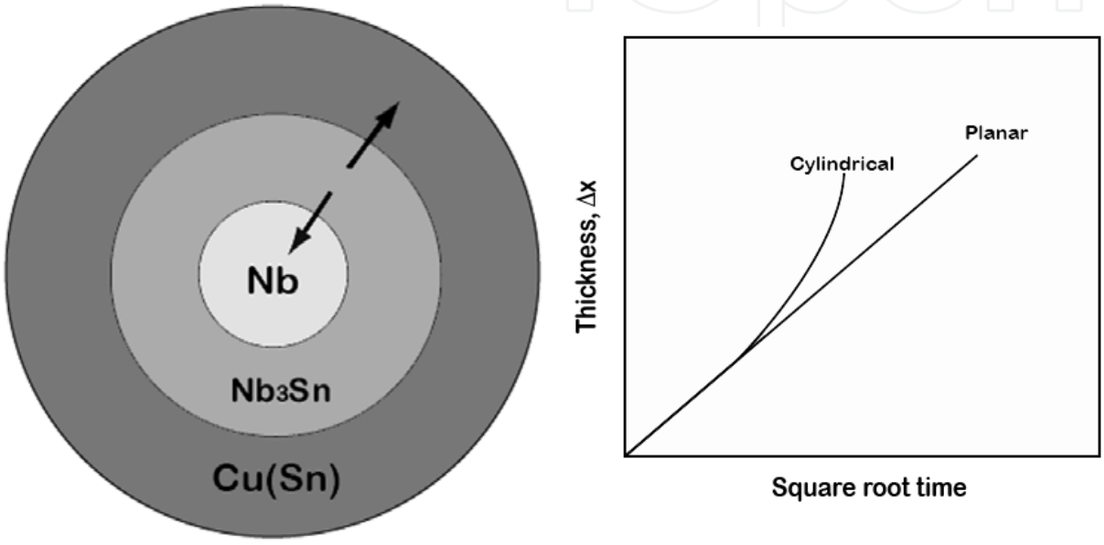

(a) (b)

Fig. 7. (a) The growth of Nb3Sn product phase in the sample with cylindrical geometry is shown. Arrows indicate the movement of the interfaces following which interfacial area changes. (b) The change in layer with square root of time in the case of sample with planar and cylindrical geometry is shown. Growth rate with planar interface will follow parabolic law in the case of diffusion controlled process; however, it will deviate in the case of growth in a sample with cylindrical geometry (van Loo, 1990).

Although Cu(Sn)/Nb diffusion couple experiment indicates that Sn is virtually only mobile species, it is rather surprising if one considers the crystal structure of the A15 Nb_3Sn intermetallic compound, as shown in Fig. 9. Sn atoms occupy the body corner and centre positions and two Nb atoms occupy each face of the cube. It can be clearly visualize that Sn atoms are surrounded by 12 Nb atoms. On the other hand, Nb atoms are surrounded by 10 Nb atoms and 4 Sn atoms. Since Nb has as its nearest neighbors Nb atoms, it can diffuse via its own sublattice if vacancies are available. In contrast, in a perfect (antisite defect free) crystal, there is no possibility for diffusion of Sn. If Sn jumps to a nearest neighbor sublattice position, it will be at a wrong place, since these sites should be occupied by Nb atoms and the jump is not allowed. However, certain amount of diffusion of Sn is still possible because of antisite and vacancies always present in the structure. According to theoretical analysis conducted by Besson et al. (Besson et al., 2007) as shown in Fig. 10a, there is a significant concentration of antisite defects in the compound, even at the stoichiometric composition.

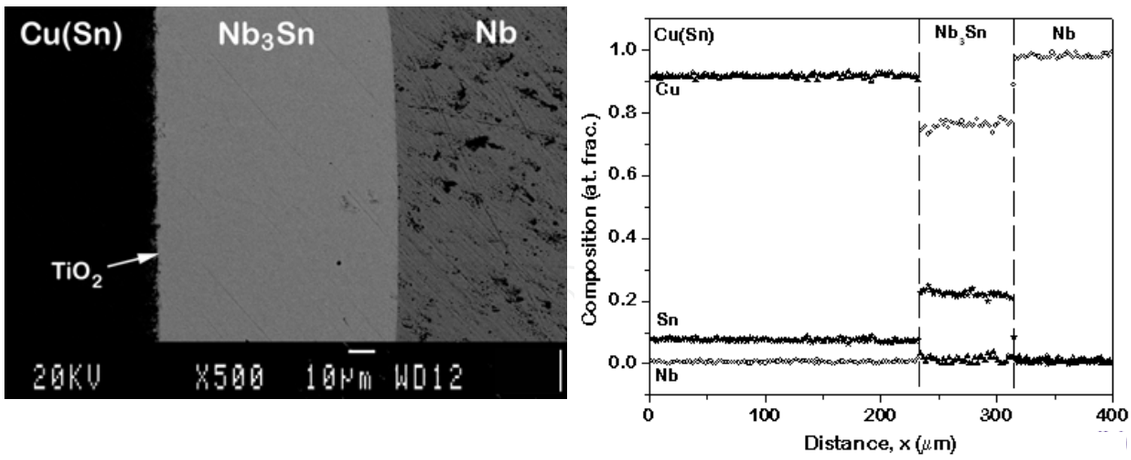

(a) (b)

Fig. 8. (a) The growth of the Nb3Sn phase and (b) corresponding composition profile are shown in a diffusion couple of Cu(8at.%Sn)/Nb at 775 °C annealed for 330 h (Kumar & Paul, 2009).

Following their calculation, the concentration of vacancies in Nb sublattice is much higher than the vacancies present in Sn sublattice. Nb can exchange position with the vacancies at its own sublattice. The presence of Nb antisite defects should further increase the diffusion rate of Nb. On the other hand, diffusion of Sn is possible only by the exchange of vacancies present on Nb sublattice with Sn antisite defects. This kind of jump is allowed since antisite Sn will move to Nb sublattice as antisite defects only. Nevertheless, the diffusion rate of Nb should always be higher than Sn in the Nb_3Sn compound, as shown in Fig. 10b based on the structural aspects alone. Of course, we are considering here only lattice diffusion. In the case of grain boundary diffusion, diffusion rate of Sn could be somewhat higher. Unfortunately, there is no experimental data available in the binary system Nb-Sn about the relative mobilities of the species in Nb3Sn phase to confirm these calculations. Till date experimental results on diffusion rates of elements are available only in two other A15 intermetallic compounds, V_3Ga (Bakker, 1985) and V_3Si (Kumar et al., 2009). In these cases, not surprisingly, diffusion rates of Ga and Si are found to be negligible compared to the diffusion rate of V. The well known Cu_3Au rule (d'Heurle & Gas, 1986) states that the if the ratio of major to minor element is equal or greater than 3 in an intermetallic compound, the major element will be the faster diffusing species. This empirical rule was developed based on the experimental data available in the literature. Hence, it is rather surprising to find that Sn is practically the only moving species in the Nb_3Sn compound growing between Nb/(Cu-Sn) diffusion couple.

Kumar and Paul (Kumar & Paul, 2009) did further experiments to study the effect of Sn content of the bronze alloy on the growth rate. Conventional diffusion couple experiments were conducted to study the growth of the phase with planar interface geometry. In a multifilamentary structure corrugated layer was always found, which resulted into a quite high standard deviation from the measured average layer thickness. Hayase & Kajihara (Hayase & Kajihara, 2006) argued that the corrugated structure is found because multifilamentary structure, which is cylindrical in geometry. They reported that the thickness of the uniform layer was similar to the one found by Kumar and Paul, as shown in Fig. 10a. However, if an uniform layer grows in a diffusion couple with a planar interface, then an uniform layer also should grow in the sample with a cylindrical geometry. The

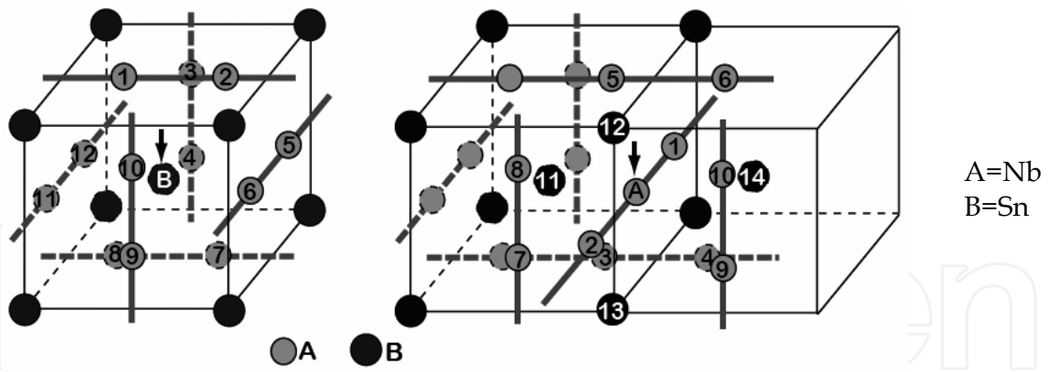

Fig. 9. A15 crystal structure is shown with the nearest neighbors of Nb and Sn.

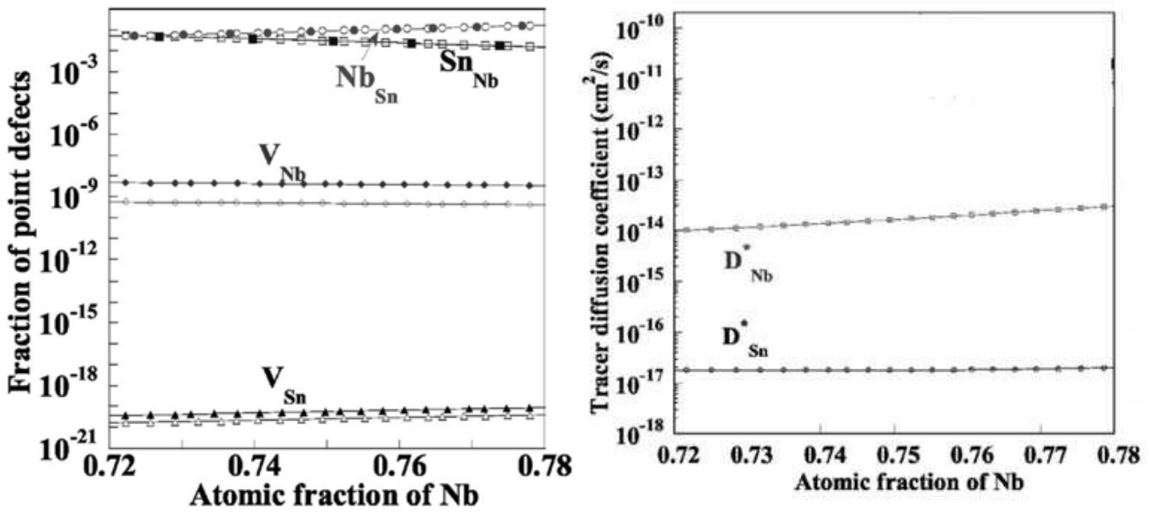

(a) (b)

Fig. 10. (a) Defect concentraions calculated by Besson et al. (Besson, 2007) in Nb_3Sn phase at 1000K. Data reported by open and closed symbols are calculated following local density approximation (LDA) and generalized gradient approximation (GDA). (b) Tracer diffusion coefficient of Nb (D^*_{Nb}) and Sn (D^*_{Sn}) calculated are shown.

radial distribution of the flux should be the same over the whole layer in the latter case. In fact, Kumar and Paul noticed that the layer grows uniform in thickness, but only locally. At different locations of the diffusion couple, large differences in the thickness of the product layer were found. As shown in the experimental results for Cu(8at.%Sn)/Nb diffusion couple annealed at 775 ^oC for 150 hrs in Fig. 11, the layer thickness varies over a wide range of 28.5-42 μm. On the otherhand, looking at one particular micrograph; it looks like Nb_3Sn phase grows more or less uniformly. In general, waviness in the product layer is found because of various reasons. For example, incubation period could be different at different places. Further, different diffusion rates because of different orientation of the grains also could cause waviness. In the present case, however, it might happen because of small inhomogeneity in the Cu(Sn) alloy. Following Farrel et al. (Farrel et al., 1974), small difference in Sn concentration can cause significant difference in the thickness of the product

layer. Despite the homogenization treatment, some inhomogeneity can still be present in the Cu(Sn) alloy, which may cause thickness variation at different locations of the diffusion couple.

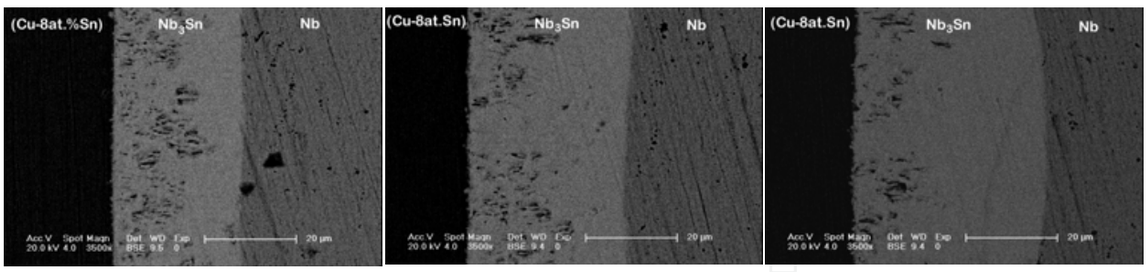

Fig. 11. Different layer thickness in the same diffusion diffusion couple annealed at 775 °C for 150 hrs at different locations is shown (Kumar and Paul, 2009).

Further the growth of the product phase for 7 and 8 at.%Sn in the Cu(Sn) alloy at different temperatures is shown in Fig. 12 a and b. The considerable deviation from the average values is evident from the standard deviation bar. It is very difficult to determine the exact

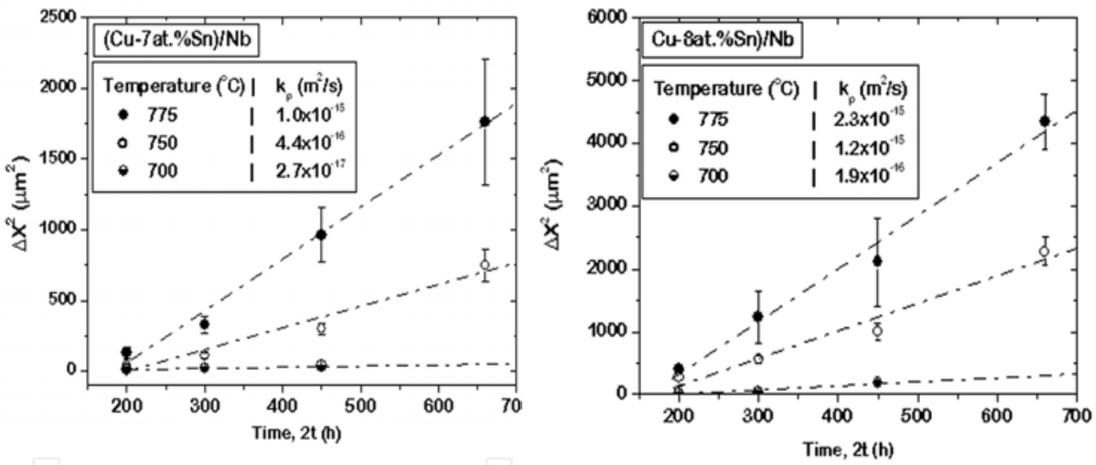

Fig. 12. The variation of layer thickness with annealing time and temperature is shown in (a) Cu(7at.%Sn)/Nb and (b) Cu(7at.%Sn)/Nb diffusion couple (Kumar & Paul, 2009).

growth exponent from these results and we have considered the parabolic growth of the phase. Following the parabolic growth constant can be calculated using

$$\left(\Delta x_{Nb_3Sn}\right)^2 = 2k_p\left(t - t_0\right) \tag{1}$$

where Δx_{Nb_3Sn} is the thickness of the Nb_3Sn phase layer and t is the total annealing time and t_0 is the incubation period. The activation energy for growth was further calculated from the Arrhenius equation

$$k_p = k_p^0 \exp\left(-\frac{Q}{RT}\right) \tag{2}$$

where k_p^0 is the pre-exponential factor, Q is the activation energy, R is the gas constant and T is the temperature in Kelvins. Fig. 13 shows the growth rate of the product phase in (Cu-7at.%Sn)/Nb and (Cu-8at.%Sn)/Nb diffusion couples at three different temperatures, 700, 750 and 775 ^oC. Following our analysis, we found that the activation energy for the growth of the phase in (Cu-7at.Sn)/Nb couple is 404 kJ/mole, whereas, in (Cu-8at.Sn)/Nb couple is 279 kJ/mole. It can be seen that there is a significant decrease in the activation energy for the diffusion along with a small change in the Sn concentration of the bronze alloy. By comparing the growth of the product phase for different Sn concentrations, as shown in Fig. 14, it was noticed that there was around 50 percent increase in the layer thickness with 1 at.% increase in the Sn concentration. In order to understand this behaviour, thermodynamic analysis was conducted to examine the change in the driving force for reactive diffusion with the change in the Sn content (Laurila et al., 2010).

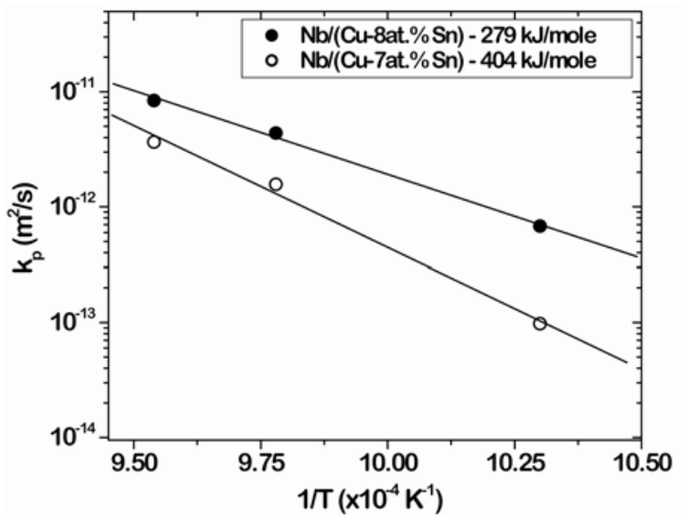

Fig. 13. The Arrhenius plot of the parabolic growth constant is shown (Kumar & Paul, 2009).

4. Thermodynamics, phase diagrams and driving force for diffusion

Thermodynamics of materials provide fundamental information both on the stability of various phases and on the driving forces for chemical reactions and diffusion processes in the system under investigation. Even though the complete (global) phase equilibrium is seldom met in practical applications, stable or metastable local or partial equilibria are generally attained at interfaces, which ensures that thermodynamics together with kinetic information provides a feasible method for analyzing the interfacial reactions in wide range of different material systems.

4.1 The Gibbs energy

The combined statement of the first and second laws of thermodynamics can be stated in terms of temperature (T) and pressure (p) with the Gibbs free energy as follows (in closed systems):

$$G \equiv U + pV - TS = H - TS \qquad 3)$$

where *U, V, H,* and *S* are the internal energy, the volume, the enthalpy and the entropy of the system, respectively. Given that $G = G(T,P,n_1, n_2,...)$ in an open system, with n_i being the number of moles of component *i*, the derivative of Eq. (1) yields:

$$dG = -SdT + Vdp + \sum_i \mu_i dn_i \tag{4}$$

where μ_i is the chemical potential of component *i*. At a constant value of the independent variables *P*, *T* and n_j $(j \neq i)$ the chemical potential equals the partial molar Gibbs free energy, $(\partial G/\partial n_i)_{P,T,j\neq i}$. The chemical potential has an important function analogous to temperature and pressure. A temperature difference determines the tendency of heat to flow from one body into another and a pressure difference on the other hand the tendency towards a bodily movement. A chemical potential can be regarded as the cause of a chemical reaction or the tendency of a substance to *diffuse* from one phase to another. This will be discussed further shortly.

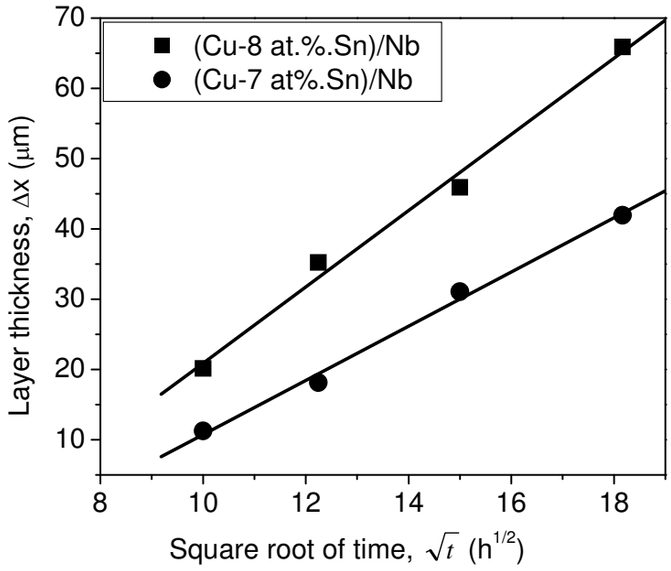

Fig. 14. The comparison between layer thicknesses at 775 °C is shown (Kumar & Paul, 2009).

With the help of the Gibbs free energy function the equilibrium state of the system can be investigated. The phase equilibria in any system are computed by summing up first all the Gibbs (free) energies of individual phases (i.e. solutions and compounds) and then minimizing - according to the second law of thermodynamics, the total energy of the system. At constant temperature and pressure the total Gibbs energy of n-component system can be written as

$$G_{tot} = \sum_{\varphi}\sum_{i}(G_i^{\varphi} n_i^{\varphi}) = \sum_{\varphi} y^{\varphi} \sum_{i=1}^{n}(x_i G_i^o + RT\sum_i^n x_i \ln x_i + G_m^E) \tag{5}$$

where y is the relative amount of a phase ϕ and x_i is a mole fraction of a component i in the system. The parameters G_i^o in Eq. 3 represent the partial molar Gibbs energies or chemical potentials of the pure components and are taken either from the SGTE databank (Dinsdale,

1991) or from the literature. G_m^E is the excess molar Gibbs energy taking into account the interactions of the constituents in all the phases to be considered.

4.2 Calculation of phase diagrams

Phase diagrams have some times been regarded as something that can only be determined experimentally. However, as phase diagram is a graphical manifestation of the state of equilibrium, it is possible to construct any kind of phase diagram if the equilibrium state of the system has been calculated. This in turn requires the evaluation of the thermodynamic properties of the corresponding system by assessing all the available experimental information in thermodynamic terms. Generally one is interested in equilibria under constant pressure and therefore the Gibbs free energy is the expedient thermodynamic function (Equation (5)). The procedure in a "nutt shell" is as follows: Analytical expressions for the free energy functions of all phases must be derived first. It is to be noted that the thermodynamic models used in the description of the Gibbs free energy of different phases are important, since successful and reliable calculation relies on the appropriate choice of model for each phase appearing in the system. Then by summing up all the Gibbs free energies of individual phases, the phase equilibria can be computed by minimizing the total Gibbs free energy of the system. The matemathical expressions for the Gibbs free energy of the individual phases contain parameters which have to be optimized to give the best fit to all the experimental information available. A major difficulty arises from the fact that the value of a parameter (which is used in the description of a simple system) will affect the evaluation of all the related higher systems. Thus, one should use as much information as possible from different sources in each optimisation process. The preceding approach is known as the CALculation of PHAse Diagrams (CALPHAD) method (Saunders & Miodownik, 1998; Kaufman & Bernstein, 1970).

The CALPHAD method is based on the axiom that complete Gibbs free energy versus composition curves can be constructed for all structures exhibited by the elements right across the whole alloy system. This involves the extrapolation of *(G,x)*-curves of many phases into regions where they are metastable and, in particular the relative Gibbs free energies for various crystal structures of the elements of the system must therefore be established. These are called as lattice stabilities and the Gibbs free energy differences between all the various potential crystal structures in which an element can exist need to be characterized as a function of temperature, pressure and volume. Information about the driving forces of different reactions in the system can also be obtained from the *(G,x)*-diagrams. This information is extremely useful, when, for example, diffusive phase growth is rationalized.

CALPHAD method is commonly used for evaluating and assessing phase diagrams. The power of the method is clearly manifested in its capability to extrapolate higher order systems from lower order systems, which have been critically assessed, thus reducing the number of experiments required to establish the phase diagram. The determination of binary equilibrium diagrams usually involves the characterization of only a few phases, and experimental thermodynamic data on each of the phases is generally available in various thermodynamic data banks as well as in the literature. However, when handling multicomponent systems or/and metastable conditions there is a need to evaluate the Gibbs free energies of many phases, some of which may be metastable over much of the composition space. Readers interested in the actual thermodynamic modelling procedures

and issues and problems associated with them are referred to vast amount of available literature, for example review articles and books (Saunders & Miodownik, 1998; Kaufman & Bernstein, 1970; Lukas et al., 2007; Ansara, 1990; Hillert, 1998).

4.3 Driving force for diffusion

The total Gibbs energy of the system can be expressed as a function of chemical potentials, which are related to the activities of the components as follows:

$$\mu_i^{\varphi} \equiv \mu_i^0(T) + RT \ln a_i \tag{6}$$

where μ_i and a_i are chemical potential and activity of element i. As explained above, the chemical potential of a component i will have the same value in all the equilibrated phases and therefore the difference in activity of a component (i.e. the driving force for its diffusion) will vanish at equilibrium. In the case of local equilibrium there are concentration gradients in the adjoining phases, but due to the chemical interaction between component atoms the diffusion is not necessarily driven by these gradients. Instead, the difference in chemical potential is the real driving force for diffusion as already discussed. A fundamental condition is that no atom can diffuse intrinsically against its own activity gradient (van Loo, 1990). If it would climb up its own activity profile, it would mean that the component moves from the region of lower chemical potential to a region of higher chemical potential – a process that does not spontaneously occur in nature. If a maximum is found experimentally in the activity profile of a component, the intrinsic movement of the other components causes it. This requirement can be used when movement of different species in a given reaction layer sequence are considered. To aid this analysis, another type of equilibrium diagrams – potential diagrams- can be utilized (Laurila et al., 2004).

5. Thermodynamic-kinetic analysis of the growth of Nb_3Sn

As already discussed there are basically three open questions concerning the growth of Nb_3Sn by the bronze technique:

1. Why Sn is the only diffusing species during the reaction?
2. Why there is such a drastic increase in the thickness of the Nb_3Sn grown under the same experimental conditions, when Sn content of the Cu(Sn) alloy is increased from 7 at.% to 8 at.%?
3. Is there solubility of Cu to Nb_3Sn?

What has been stated earlier indicates the thermodynamic-kinetic approach can be utilized to find answers to the above three questions.

With the aim to calculate the thermodynamic parameters to understand the diffusion process, the ternary phase diagram of the Cu-Nb-Sn system is calculated with the help of the assessed data from the references (Hämäläinen et al., 1990; Toffolon et al., 2002; Shim et al.,1996). In these calculations, all intermetallic compounds are modeled as binary compounds, since dissolution of ternary elements are found to be negligible based on the available information. In addition, no ternary compounds are known to exist in the Cu-Nb-Sn system. Isothermal section calculated at 700 °C is shown in Fig. 15. It is in general consistent with the very recent publication on the thermodynamic assesment of the Cu-Nb-Sn system (Li et al., 2009), except for two details. Firstly, in (Li et al., (2009) the Nb_6Sn_5 phase is stable already below 700 °C, different from our calculations and results of (Pan et al, 1980).

Secondly, there is also some ternary solubility to both Nb_3Sn and Nb_6Sn_5 in the diagram in (Li et al., 2009) contrary to our results and results by (Yamashina & Kajihara, 2006).

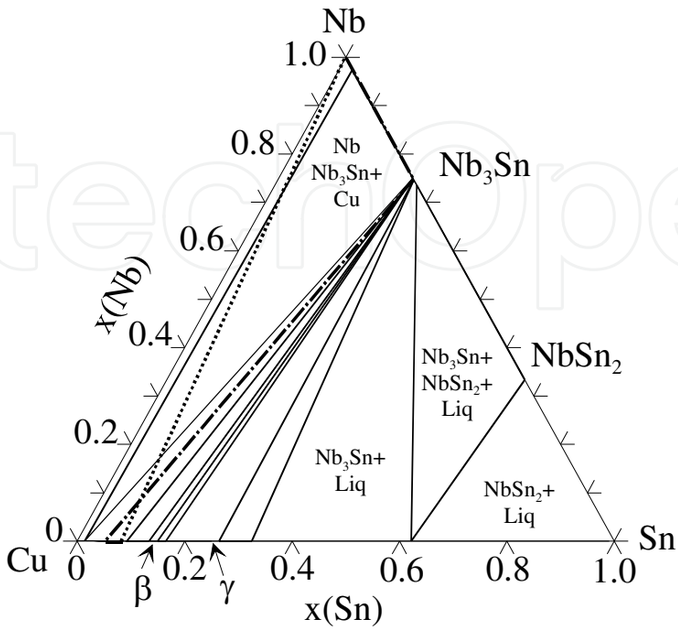

Fig. 15. Calculated Cu-Nb-Sn isothermal section at 700 °C. Dotted line is the contact-line (C.L.) between the end-members and the dashed-dotted line shows the diffusion path.

However, as the most relevant equilibrium to our analysis is the three-phase triangle Cu-Nb_3Sn-Nb, the occurrence of Nb_6Sn_5 phase that establishes equilibrium with the liquid phase, has no effect on the equilibria between Nb_3Sn and Cu, β or γ phases, even if it is stable already at 700 °C or below. Further, we have also induced ternary solubility to Nb_3Sn (up to 10 at.%) and it did not have any effect on the three-phase triangle of interest (Fig. 16) and did not markedly influence the values of chemical potentials of the species. Thus, from our analysis point of view these minor differences can be disregarded. With the same set of assessed thermodynamic data the values of driving forces for the diffusion (the difference in chemical potential between two moving interfaces, $\Delta\mu$ in the diffusion couple) of given species over Nb_3Sn layer at 700 °C, 750 °C and 775 °C, as a function of Sn content of 6, 7 and 8 at.% in Cu-Sn alloy were calculated. The results (interface I is Cu(Sn)/Nb_3Sn and interface II is Nb_3Sn/Nb) are tabulated in Table I. Following the data on driving force, it is clear that only the diffusion of Sn through the product layer is allowed from the thermodynamic point of view. If Nb or Cu would diffuse intrinsically they should move against their own activity gradient, which is not possible (van Loo, 1990). Now if we reconsider the possible atomic mechanism of diffusion, as discussed previously, the diffusion of Nb should be much easier than diffusion of Sn. However, from the thermodynamic point of view there is no possibility of diffusion of Nb (and Cu) in Nb_3Sn in Nb/Cu(Sn) diffusion couple, as there is no driving force. Thus, the only way for the product layer to grow is by diffusion of Sn. That is also the reason why the TiO_2 particles used as inert markers are found near the Cu(Sn)/Nb_3Sn interface. The fact that Sn must be the only *intrinsically* diffusing species in this reaction layer sequence, from the thermodynamic point of view, is evident also based on the isothermal section shown in Fig. 15, which shows also the diffusion path for the reaction

sequence under investigation. When we have a diffusion couple Cu(Sn)/Nb (the contact line connecting the end-members is drawn as dashed line) the diffusion path must proceed as drawn in Fig. 15. This is because of the requirement that the contact line between the end-members must be crossed at least once; as otherwise, the mass balance would not be fulfilled (van Loo, 1990). Thus, as can be seen from the figure, the diffusion path must always start from the Cu(Sn) end *towards* the Cu corner (i.e. towards higher activity of Cu) and then go to Nb_3Sn and finally to Nb. This also means that there should not be Cu inside Nb_3Sn, as in order to get there, it would have to move against its own activity gradient. Yamashina et al. (Yamashina & Kajihara, 2006) also calculated the activity diagram for Sn diffusion and concluded that the reaction product layer sequence can be produced by diffusion of Sn along its lowering activity, consistent with the present analysis. However, as they did not calculate the activity values for the other two component, they could not provide the reasons for the absence of movement of Nb and Cu.

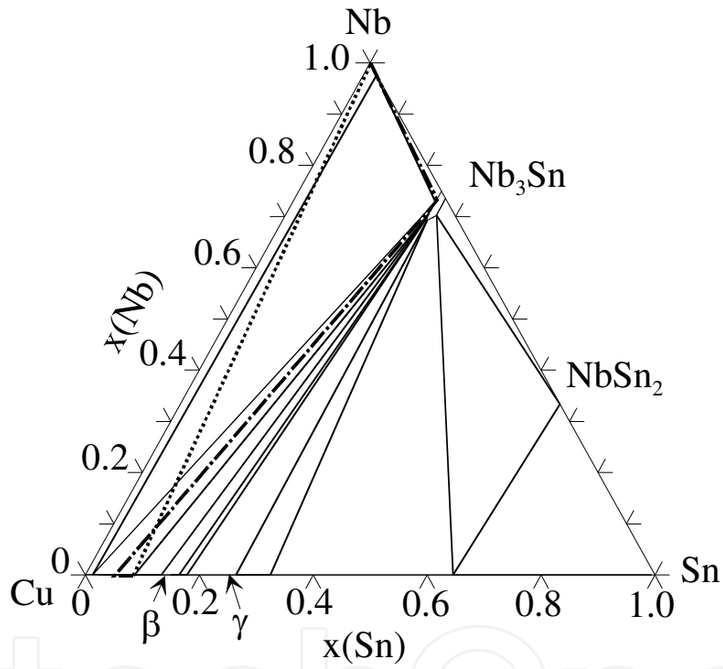

Fig. 16. Calculated Cu-Nb-Sn isothermal section at 700 °C, with 10 at-% Cu solubility induced to Nb_3Sn. Dotted line is the contact-line (C.L.) between the end-members and the dashed-dotted line shows the diffusion path.

Further from the experimental results, we have seen that there is considerable increase in the growth rate and decrease in activation energy just because of small increase in Sn content from 7 to 8 atomic percent in the Cu-Sn alloy. It does not look as surprising, when we consider the change in chemical potential between the two interfaces in the diffusion couple owing to the change in the Sn content. For example at 775 ^{o}C, the difference in the chemical potential of Sn changes from -14217 in Nb/(Cu-7at.%Sn) couple to -16008 J/mole in Nb/(Cu-8at.%Sn) at the same temperature. The change is around 12.5%. We can roughly consider that the flux of elements is linearly proportional to the driving force, if we neglect any other differences in the properties of the end members, which might be caused by the change in the Sn content. Thus we can estimate that the amount of Sn flux through the product layer (Nb_3Sn) will increase

approximately by 12.5%. Further, since one mole of Sn produces four moles of the product layer, we can expect that there will be at least 50% increase in the layer thickness because of the change in Sn content from 7 to 8 at.%. The results presented in the Fig. 14 are consistent with this calculation. So the increase in layer thickness because of such a small change in Sn content in the (Cu-Sn) alloy does not look surprising from the thermodynamic point of view. Since the change in driving force plays an important role in the activation energy, the considerable change in activation energy because of the change in Sn content is also rational. Consequently the high value of activation energy for the growth of Nb_3Sn is also acceptable, since it occurs by diffusion of Sn, which is dependent on the concentrations of antisite defects and vacancies present in the structure.

Temperature (°C)	Sn at.% in Cu(Sn) alloy	$\Delta\mu_{Sn}^{I\to II}$ (J/mol)	$\Delta\mu_{Cu}^{I\to II}$ (J/mol)	$\Delta\mu_{Nb}^{II\to I}$ (J/mol)
700	6	-15498	508	5634
	7	-17391	639	5765
	8	-19101	777	6336
750	6	-13464	487	4489
	7	-15402	621	5136
	8	-17150	762	5719
775	6	-12226	457	4076
	7	-14217	591	4740
	8	-16008	733	5338

Table I. The difference in chemical potential of elements between two different interfaces is listed.

6. Effect of alloying elements

There is always a demand to increase the critical temperatures, T_c, the critical current density, J_c, and the upper critical magnetics field, H_{c2}. It has been found that addition of alloying elements, such as, Ga, Ti, Ta, Zr, Hf etc. facilitates the use of the Nb_3Sn superconductor above 12 T (Sekine et a., 1979). The addition of around 3 at.% Ti to Nb increases the maximum critical current density measured at 20 T and at 1.8 as well as at 4.2 K. The addition of Ti in Nb is also found to increase the layer thickness of the product phase. Moreover, the Ti content of the Nb_3Sn is found to be more or less the same as the Ti content in the Nb alloy. Ta also has the same beneficial role and the maximum J_c was found with 4-5 at.%Ta in the Nb core (Suenaga et al. 1984). However, T_c decreases along alloying and with much faster rate because of Ti than Ta. Many times both Ti and Ta are added together to achieve maximum benefit (Flükiger et al., 2008). It was noticed that addition of Ga at the cost of Sn increases J_c, however, the growth rate of the product phase decreases (Dew-Hughes, 1977, Horigami et al., 1976, Sekine et al., 1979, Sekine et al. 1981). It is probable that because of the decrease of Sn content in the alloy, the activity of Sn is lowered, accordingly the driving force for the diffusion through the Nb_3Sn layer is diminished and thus the growth rate is decreased. It was also noticed that the addition of Hf and Zr in the Nb core increases both J_c and the growth rate of Nb_3Sn (Sekine et al., 1979, Sekine et al. 1981).

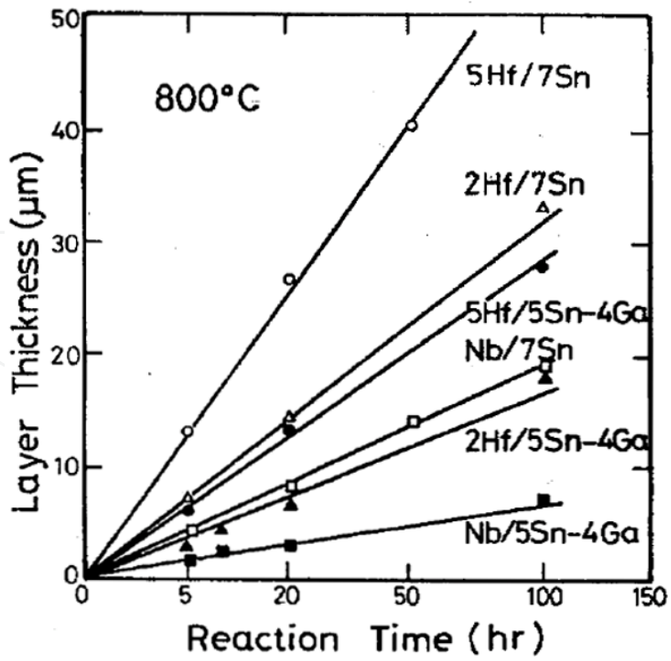

Fig. 17. The increase in layer thickness with the increase in annealing time at 800 °C with different Nb core and matrix Cu(Sn) bronze alloy is shown. Zr and Hf are added to the core and Ga is added to the matrix. 5Hf/7Sn means Nb-5at.%Hf/Cu-7at.%Sn (Sekine et al., 1981).

Sekine et al., 1981 and Takeuchi et al., 1981 studied the effect of addition of Ti, Zr and Hf in the Nb core and Ga in the Cu(Sn) matrix. The results reported in (Sekine et al., 1981) are shown in Fig. 17. It can be seen clearly that Ga addition at the cost of some Sn content decreases the growth rate of the product phase, although the content of (Sn+Ga) is higher than the Sn content of the bronze alloy without Ga. On the other hand, the addition of Hf increases the growth rate of the product phase drastically. The examination on grain structure revealed grain coarsening because of addition of Ga. On the other hand there was hardly any difference in the average grain size because of addition of Hf. Takeuchi et al., (Takeuchi et al., 1981), published a paper with similar studies and examined the effect of Ga content in the Cu(Sn) bronze alloy and Ti, Zr and Hf in the Nb core. They noticed that the addition of Zr and Hf beyond 10 and 5 at.%, respectively, created difficulties in workability to draw the material as a thin wire. The growth of the product phase with all investigated compositions was found to be parabolic with time, at least during the initial stage. Like in (Sekine et al., 1981; Takeuchi et al., 1981) they also found that there is a decrease in the growth rate because of Ga addition. However, the layer thickness increased considerably when Ti, Zr and Hf were added to the Nb core, as shown in Fig. 18. Composition analysis indicates that the Ti content in the Nb_3Sn phase was higher than that of the other elements. A Ga-rich phase was found to appear when Ga content was increased to 9 at.%. Likewise a Zr content of more than 5 at.% produced precipitates of Zr rich phase inside the Nb_3Sn phase. Close examination of the grain structure indicated the presence of finer grains because of addition of Ti, Zr and Hf. The grain structure did not change much with the increase of the alloying element content beyond 2 at.%. Ga addition, on the other hand, causes significant grain coarsening, as seen also in (Sekine et al., 1981 and Takeuchi et al., 1981).

Tachikawa et al. (1991) studied the effect of addition of Ge in the bronze alloy. They considered pure Nb and alloyed with Ta, Ti and Hf core. They found significant increase in the critical current density because of Ge addition. Grain refinement could be the reason to increase in J_c, however, the change in layer thickness because of addition of Ge is not reported.

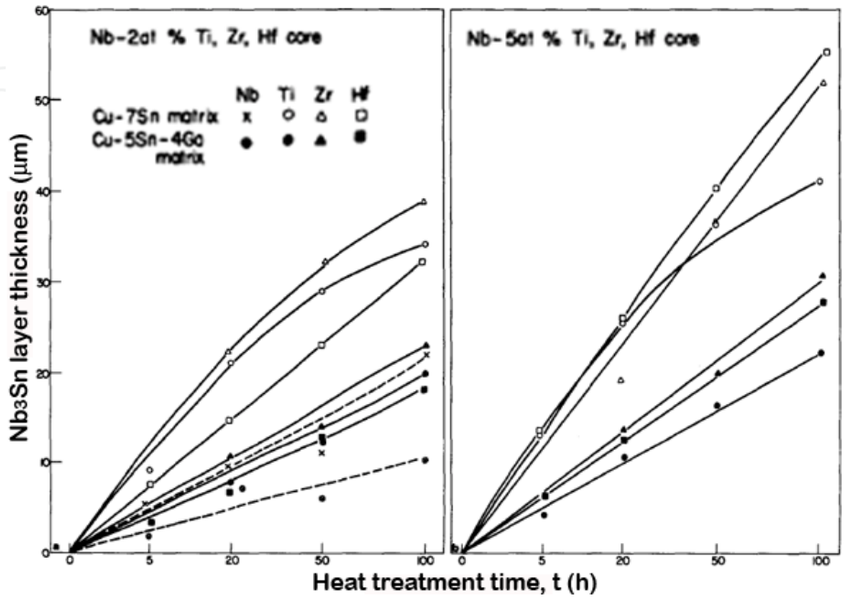

Fig. 18. The increase in layer thickness with the increase in annealing time at 800 °C is shown. (a) Nb-2at.%Ti, Zr and Hf core (b) Nb-5at.%Ti, Zr and Hf core (Takeuchi et al., 1981).

7. Conclusive remarks

It is clear from the results reported in various articles that it is very difficult to draw any definite conclusion about the growth and diffusion mechanism in Nb_3Sn based on the results available in the literature. It was found that the growth exponent is typically close to 0.5, when Sn content in the bronze alloy is relatively high. With the decrease in Sn content growth exponent deviates from this and this indicates that some other factors become important. Kirkendall marker experiments conducted by Kumar and Paul (2009) clearly indicated that Sn is almost the only mobile species. Further, very minor amount of Cu (Suenaga and Jansen, 1983) was found in the Nb_3Sn product phase and no Sn was found in Nb. Although thermodynamic analysis explains that there is no driving force for Cu to diffuse through the product layer, the trace amount of Cu was in mainly in grain boundaries (Suenaga and Jansen, 1983). There is always a chance that some amount could be added as impurity. It is quite possible that when Sn content is high in the Cu(Sn) bronze alloy, the process is controlled by the diffusion of Sn through the Nb_3Sn. At the later stage of the annealing or when the Sn content is initially low, the diffusion process may become much complicated because of lack of availability of Sn. Then the growth exponent could increase as was found in (Reddi et al., 1983).

Farrel et al. (1974 & 1975) argued that the growth of the Nb_3Sn phase mainly occurs because of grain boundary diffusion and developed a model to explain the diffusion process. They developed this model based on the growth exponent they calculated, which was found to

0.35 and the activation energy for growth, which was found to be 51.9 kJ/mol. However other researchers (Larbalestier et al. 1975; Reddi et al., 1983; Kumar & Paul, 2009) found much higher activation energy values (above 200 kJ/mol). It is in fact very difficult to find the exact diffusion mechanism from this kind of experiments. What we actually measure, is the apparent diffusion coefficient, which is a kind of average from the contribution from lattice and grain boundary diffusion. Nevertheless, the relatively high activation energy clearly indicates that there must be significant contribution from lattice diffusion. This might be the reason that even though Takeuchi et al. 1981 found that after addition of Ti, Zr and Hf beyond a certain limit did not change the grain morphology, however, there was significant increase in the growth rate. There might be significant increase in the driving force for diffusion with the increase in alloy content and there could also be increase in defect concentration (vacancies and antisites). However, further understanding is lacking because of unavailability of these information at the present. Further dedicated study is required to develop better understanding especially the effect of alloy additions on the growth of the product phase.

8. References

Adda, Y. and Philibert, J. (1981). *Atom movements and mass transport in solids*. Les Ulis: Les Éditions de Physique, 1991.

Ansara I.(1990). Thermodynamic modelling of solution phases and phase diagram calculations, *Pure Applied Chemistry*, **62**, (1990), 71-78.

Bakker H., *Diffusion in Solids: Recent developments*, edited by Dayananda MA and Murch GE. The Metallurgical society publication, Warrendale, PA (1985) 39-63.

Besson, R., Guyot, S. & Legris, A., Atomic scale study of diffusion in A15 Nb_3Sn. (2007) *Physical Review B* Vol. 75 (2007) 0541051- 0541057

Dew-Hughes, D. (1977) Effect of third element additions on the properties of bronze processed Nb_3Sn. *IEEE Transactions on Magnetics* Vol. 13 (1977) 651-654.

d'Heurle, FM., and Gas, P., (1986). Kinetics of formation of silicides: A review. *Journal Materials Research* Vol. 1 (1986) 205-221

Dinsdale A.T. (1991). SGTE data for pure elements, *Calphad*, **15,** (1991), 317-425.

Easton, DS. & Kroeger, DM. (1979). Kirkendall voids-A detriment to Nb_3Sn superconductors. *IEEE Transactions on Magnetics* Vol. 15 (1979) 178-181

Farrel, HH., Gilmer, GH. & Suenaga M. (1974) Grain boundary diffusion and growth of intermetallic layers:Nb_3Sn. *Journal of Applied Physics* Vol. 45 (1974) 4025-4035.

Farrel, HH., Gilmer, GH. & Suenaga M. (1975) Diffusion mechanisms for the growth of Nb_3Sn intermetallic layers. *Thin Solid Films* Vol. 25 (1975) 253-264.

Flükiger, R., Uglietti, D., Senatore, C. & Buta, F. (2008) Microstructure, composition and critical current density of superconducting Nb3Sn wires. *Cryogenics* Vol. 48 (2008) 293-307.

Hämäläinen M., Jaaskelainen K., Luoma R., Nuotio M., Taskinen P., and Teppo O, (1990). A thermodynamic analysis of the binary alloy systems Cu-Cr, Cu-Nb and Cu-V, *Calphad*, Vol. 14 (1990) 125-137.

Harrison, LG. (1961). Influence of dislocations on diffusion kinetics in solids with particular reference to the alkali halides *Transaction of Faraday Society* Vol. 57 (1961) 1191-1199.

Hayase, T. & Kajihara, M. (2006). Kinetics of reactive diffusion between Cu-8.1Sn-0.3Ti alloy and Nb. *Materials Science and Engineering A*, Vol. 433 (2006) 83-89.

Hillert M. (1998). *Phase Equilibria, Phase Diagrams and Phase Transformations : Their Thermodynamic Basis*, Cambridge Univ. Press, (1998).

Horigami, O., Luhman, T., Pande, CS. & Suenaga, M. (1976) Superconducting properties of $Nb_3(Sn_{1-x}Ga_x)$ by a solid-state diffusion process. *Applied Physics Letters* Vol. 28 (1976) 738-740.

Kaufman L. and Bernstein H. (1970). *Computer Calculation of Phase Diagrams*, Academic Press, New York, (1970).

Kumar, AK. & Paul, A. (2009) Interdiffusion and growth of the superconductor Nb_3Sn in Nb/Cu(Sn) diffusion couples. *Journal of Electronic Materials* Vol. 38 (2009) 700-705.

Kumar, AK., Laurila T., Vuorinen, V. and Paul, A. (2009). Determination of diffusion parameters and activation energy of diffusion in V_3Si phase with A15 crystal structure. *Scripta Materialia* vol. 60 (2009) 377-380.

Larbalestier, DC., Madsen, PE., Lee, JA., Wilson, MN., & Charlesworth, JP. (1975) Multifilamentary niobium tin magnet conductors. *IEEE Transactions on Magnetics* Vol. 11 (1975) 247-250.

Laurila, T., Vuorinen, V., Kumar, AK. & Paul A. (2010). Diffusion and growth mechanism of Nb_3Sn superconductor grown by bronze technique, *Applied Physics Letters* Vol. 96 (2010) 231910

Laurila T., Vuorinen V., and Kivilahti J.K. (2004). Analyses of interfacial reactions at different levels of interconnection, *Materials Science in Semicond. Processing* Vol. **7** (2004), 307-317.

Lee, PJ. & Larbalestier DC. (2001). Compositional and microstructural profiles across Nb3Sn filaments produced by different fabrication methods. *IEEE Transactions on Applied Superconductivity*. Vol. 11 (2001) 3671-3674.

Lee, PJ. & Larbalestier DC. (2005) Microstructure, microchemistry and the development of very high Nb_3Sn layer critical current density. *IEEE Transaction of Applied Superconductivity* Vol. 15 (2005) 3474-3477.

Lee, PJ. & Larbalestier DC. (2008). Microstructural factors important for the development of high critical current density Nb3Sn strand. *Cryogenics* Vol. 48 (2008) 283-292.

Li M., Du Z., Guo G. and Li C., (2009). Thermodynamic Optimization of the Cu-Sn and Cu-Nb-Sn Systems, *Journal Alloys Compounds* Vol. 477 (2009) 104-117.

Lukas H., Fries S., and Sundman B. (2007). Computational Thermodynamics- The Calphad Method, *Cambridge University Press* (2007).

Müller, H. & Schneider Th. (2008). Heat treatment of Nb_3Sn conductors. *Cryogenics* Vol. 48 (2008) 323-330.

Muranishi, Y. & Kajihara, M. (2005) Growth behavior of Nb3Sn layer during reactive diffusion between Cu-8.3Sn alloy and Nb. *Materials Science and Engineering A* Vol. 404 (2005) 33-41.

Pan V., Latysheva V., Litvinenko Y., Flis V. and Gorskiy V., (1980). The Phase Equilibria and Superconducting Properties of Niobium-Tin-Copper Alloys, The Physics of Metals and Metallography Vol. 49 (1980) 199-202.

Reddi, BV., Raghavan, V., Ray, S. & Narlikar, AV. (1983) Growth kinetics of monofilamentary Nb_3Sn and V_3Ga synthesized by solid-state diffusion. *Journal of Materials Science* Vol. 18 (1983) 1165-1173.

Saunders N. and. Miodownik A.P., (1998). CALPHAD, *Calculation of Phase Diagrams*, Pergammon Materials Series, Elsevier Science, (1998).

Sekine, H., Tachikawa, K. & Iwasa, Y. (1979). Improvements of current-carrying capacities of the composite-processed Nb_3Sn in high magnetic fields. *Applied Physics Letters* Vol. 35 (1979) 472-473.

Sekine, H., Takeuchi, T. and Tachikawa, K. (1981) Studies on the composite processed Nb-Hf/Cu-Sn-Ga high-field superconductors. *IEEE Transactions on Magnetics* Vol. 17 (1981) 383-386.

Sharma, RG. (1987). Review on the fabrication techniques of A-15 superconductors. *Cryogenics*, Vol. 27 (1987) 361-377

Shim J.H., Oh C.S., Lee B.J., Lee D.N., (1996). Thermodynamic Assessment of the Cu-Sn System, *Z Metallkunde* Vol. 87 (1996) 205-212.

Suenaga M. & Jansen W. (1983) Chemical compositions at and near the grain boundaries in bronze processed superconducting Nb_3Sn. *Applied Physics Letters* Vol. 43 (1983) 791-793.

Suenaga, M. & Jansen, W. (1983). Chemical compositions at and near the grain boundaries in bronze processed superconducting Nb3Sn. *Applied Physics Letters* Vol. 43 (1983) 791-793.

Suenaga, M. (1981) *Superconductor Materials Science: Metallurgy Fabrication and Applications*, Edited by Foner S. & Schwartz BB. Plenum, New York (1981) pp. 201

Suenaga, M., Tsuchiya, K. & Higuchi, N. (1984). Superconducting critical current density of bronze processed pure and alloyed Nb3Sn at very high magnetic fields (up to 24 T). *Applied Physics Letters* Vol. 44 (1984) 919-921.

Suenaga, M., Welch, D.O., Sabatini, RL., Kammere, OF. & Okuda, S. (1986). Superconducting critical temperatures, critical magnetic fields, lattice parameters and chemical compositions of "bulk" pure and alloyed Nb_3Sn produced by bronze process. *Journal of Applied Physics*, Vol. 59 (1986) 840-853.

Tachikawa, T., Terada, M., Endo, M. & Miyamoto, Y. (1992). Bronze processed Nb_3Sn with addition of Germanium to matrix. *Cryogenics* Vol. 33 (1993) 205-208.

Takeuchi, T., Asano, T., Iijima, Y. & Tachikawa, K. (1981). Effects of the IVa element addition on the composite-processed superconducting Nb_3Sn. *Cryogenics* Vol. 21 (1981) 585-589.

Toffolon C., Servant C., Gachon J. C., and Sundman B., (2002). Reassessment of the Nb-Sn system *Journal of Phase Equilibria*, 23, (2002) 134-139.

Van Loo, FJJ. (1990). Multiphase difusion in binary and ternary solid state systems. *Progress in Solid State Chemistry* Vol. 20, (1990) 47-99

Yamashina T. and Kajihara M., (2006). Quantitative Explanation for Uphill Diffusion of Sn During Reactive Diffusion Between Cu-Sn Alloys and Nb, *Materials Transaction* Vol. 47 (2006), 829-837.

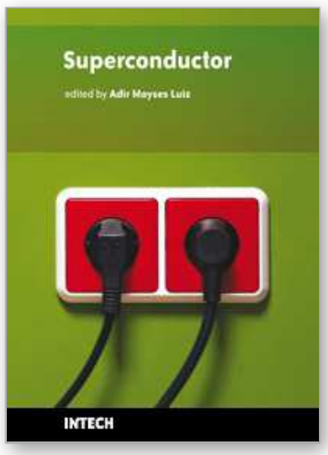

Superconductor
Edited by Doctor Adir Moyses Luiz

ISBN 978-953-307-107-7
Hard cover, 344 pages
Publisher Sciyo
Published online 18, August, 2010
Published in print edition August, 2010

This book contains a collection of works intended to study theoretical and experimental aspects of superconductivity. Here you will find interesting reports on low-Tc superconductors (materials with Tc< 30 K), as well as a great number of researches on high-Tc superconductors (materials with Tc> 30 K). Certainly this book will be useful to encourage further experimental and theoretical researches in superconducting materials.

How to reference
In order to correctly reference this scholarly work, feel free to copy and paste the following:

Aloke Paul, Tomi Laurila and Vesa Vuorinen (2010). Microstructure, Diffusion and Growth Mechanism of Nb3Sn Superconductor by Bronze Technique, Superconductor, Doctor Adir Moyses Luiz (Ed.), ISBN: 978-953-307-107-7, InTech, Available from: http://www.intechopen.com/books/superconductor/microstructure-diffusion-and-growth-mechanism-of-nb3sn-superconductor-by-bronze-technique

INTECH
open science | open minds

InTech Europe
University Campus STeP Ri
Slavka Krautzeka 83/A
51000 Rijeka, Croatia
Phone: +385 (51) 770 447
Fax: +385 (51) 686 166
www.intechopen.com

InTech China
Unit 405, Office Block, Hotel Equatorial Shanghai
No.65, Yan An Road (West), Shanghai, 200040, China
中国上海市延安西路65号上海国际贵都大饭店办公楼405单元
Phone: +86-21-62489820
Fax: +86-21-62489821

IntechOpen